European Congress on Computational Methods in Applied Sciences and Engineering
ECCOMAS 2000
Barcelona, 11-14 September 2000

DNS OF TURBULENT FLOW AND HEAT TRANSFER IN A CHANNEL WITH SURFACE MOUNTED CUBES

R.W.C.P. Verstappen, R.M. van der Velde† and A.E.P. Veldman

Research Institute for Mathematics and Computer Science
University of Groningen, P.O.Box 800, 9700 AV Groningen, The Netherlands.
Email: verstappen@math.rug.nl, veldman@math.rug.nl; web: http://www.math.rug.nl/
†Present address: TNO Bouw, MIT/NM, Building 33, P.O.Box 49, 2600 AA Delft,NL.

Key words: Direct Numerical Simulation, Turbulent Flow, Heat Transfer, Channel Flow; Wall-Mounted Obstacles, Higher-Order, Symmetry-Preserving Discretisation.

Abstract. *The turbulent flow and heat transfer in a channel with surface mounted cubical obstacles forms a generic example of a problem that occurs in many engineering applications, for instance in the design of cooling devices. We have performed a numerical simulation of it without using any turbulence models. This approach is the most accurate - but also the most expensive - way of computing complex turbulent flows since all dynamically significant scales of motion are to be solved numerically from the unsteady, incompressible Navier-Stokes equations and the energy equation. In view of the computational complexity, our first concern is to reduce the computational cost as far as we can get. We discretise convective and diffusive operators such that their spectral properties are preserved, i.e. convection ↔ skew-symmetric; diffusion ↔ symmetric, positive definite. Such a symmetry-preserving discretisation is stable on any grid and conserves mass, momentum and kinetic energy if the dissipation is turned off. First, the results of a second-order and a fourth-order, symmetry-preserving discretisation are compared for a fully developed, turbulent flow in a plane channel. The more accurate fourth-order method is applied to perform a numerical simulation of turbulent flow and heat transfer in a channel, where a matrix of cubes is mounted at one wall. Here, the temperature is treated as a passive scalar. The Reynolds number (based on the channel width and the mean bulk velocity) is equal to* $Re = 13,000$. *The results of the numerical simulation agree well with the available experimental data.*

1 INTRODUCTION

The turbulent flow and heat transfer in a channel with surface mounted cubical obstacles forms a generic example of a problem that occurs in many engineering applications, for instance in the design of cooling devices. It formed one of the test cases at the last three ERCOFTAC/IAHR/COST Workshops on Refined Turbulence Modelling. See [1], [2] and [3]. From this series of workshops it may be concluded that this test case provides a major challenge to current Reynolds-averaged Navier-Stokes (RaNS) models. At present, it poses a problem to which no RaNS model seems to have a satisfactory answer.

We have performed a numerical simulation of it without using any turbulence models. This approach is the most accurate - but also the most expensive - way of computing complex turbulent flows since all dynamically significant scales of motion are to be solved numerically from the unsteady, incompressible Navier-Stokes equations and the energy equation. Here, the energy equation is considered in the Boussinesq approximation, *i.e.* the temperature can be computed as a passive scalar. The Reynolds number is equal to 13,000 (based on the channel width and the mean bulk velocity); the Prandtl number equals 0.71 (air).

In view of the computational complexity, our first concern is to reduce the computational cost as far as we can get. This implies, among others, that the number of grid points has to be kept as small as possible. To use the lowest possible number of grid points, spatial discretisation methods for the Navier-Stokes equations need to be strained to their limit. On non-uniform grids various ways exist to discretise convective and diffusive operators. We propose to apply a high-order discretisation method that preserves the spectral properties of the convective and diffusive operators. That is, the coefficient matrix of the discrete convective operator is skew-symmetric and diffusion is represented by a symmetric, positive-definite coefficient matrix. In this way, the mass, momentum and kinetic energy of the resulting symmetry-preserving discrete system are conserved if the physical dissipation is turned off.

Traditionally, discretisation methods are selected on basis of their local truncation error. The questioning of the cost-effectiveness of discretisation schemes for turbulent flow simulations has led to methods with a higher-order local truncation error. When discretisation methods are constructed by minimizing the local truncation error, the skew-symmetry of the convective term is easily lost, and quantities that are to be conserved, like the kinetic energy, are not conserved. Consequently, an unconditionally stable solution cannot be obtained, unless artificial damping is added [4]. This has been our main motivation to investigate the symmetry-preserving discretisation approach.

On a (staggered) uniform grid, the second-order scheme of Harlow and Welsh [5] preserves the symmetries of the convective and diffusive operator, and thus conserves the mass, momentum and energy of an inviscid flow. Harlow and Welsh's scheme forms the basis of our approach. We generalise their scheme to non-uniform meshes in such a manner that the symmetries are not broken, and improve its order of accuracy by means of

a Richardson extrapolation, as in [6]. Recently, Morinishi *et al.* [7] have used another way of making higher-order discretisation schemes. For uniform grids, our scheme is identical to their fully-conservative scheme (Eq. (101) in [7]). Yet, for non-uniform meshes Morinishi *et al.* follow a different approach. They extend their scheme to non-uniform meshes by adapting the weights in the difference operators to the local grid spacings. This breaks the symmetry, and consequently the resulting scheme does not (fully) maintain the conservation properties.

In this paper, we will derive a symmetry-preserving discretisation and show how well it performs for a complex turbulent flow with heat transfer. Therefore we will compare the results of the numerical simulation with the available experimental data. In addition to that, we aim to add insight into the physics of the problem under consideration.

The paper is organised as follows. The mathematical model is concisely presented in Section 2. The numerical approach is described in Section 3. Numerical results are discussed in Section 4.

2 PROBLEM DESCRIPTION

A matrix of 25×10 cubes (each of size h^3) is mounted at one wall of the channel. The pitch of the cubes equals $4h$, both in the streamwise and in the spanwise direction. The height of the channel is $3.4h$. Flow measurements by Meinders [8] around the middlemost cube at the 18th row from the inlet showed that the influence of the in- and outlet can be neglected there: a fully developed, symmetrical state was observed there. This justifies to confine the flow domain to a sub-channel unit of dimension $4h \times 3.4h \times 4h$ with periodic boundary conditions in the streamwise and in the spanwise direction. Figure 1 displays a sub-channel unit.

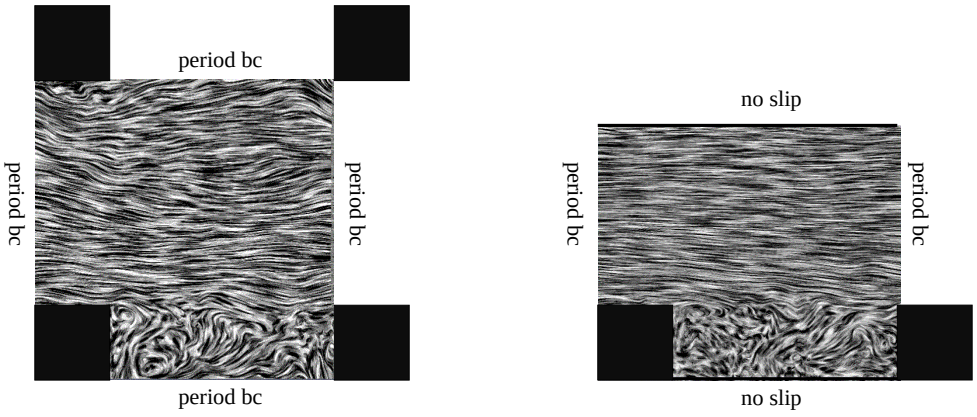

Figure 1: Top- and side-view of a sub-channel unit. Both pictures show an instantaneous flow field (taken from the DNS) at the plane that bisects the cubes. The flow is directed from left to right.

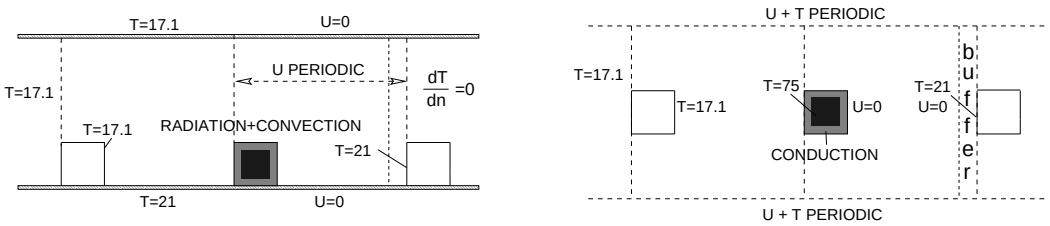

Figure 2: An overview of the boundary conditions. The left hand side picture shows a side-view of the channel; the right hand side displays a top-view.

For the heat transfer we have doubled the domain in the streamwise direction, since only one cube in the array is heated in the experiment by Meinders *et al.* [9]. The inlet is taken $4h$ upstream from the heated cube (see Figure 2). The heated cube is made of a copper core covered by an epoxy layer of thickness $h/10$. The temperature in the epoxy layer is governed by an unsteady diffusion equation. The fluid and cube temperature are equal at the five faces of the cube that are cooled by the fluid flow. The cube heats the fluid by radiation and conduction. In addition, in a small buffer zone the Prandtl number is decreased from 0.71 to 0.2 to suppress non-physical waves which may be reflected by the artificial outflow boundary.

3 SYMMETRY-PRESERVING DISCRETISATION

The sub-channel unit (shown in Figure 1) is covered by a 100^3 staggered grid that is stretched away from both the cubes and the channel walls. The first grid point away from a cube (or a wall) is located at $0.006h$. A cube is represented by 40 grid points in each direction. The grid is continued inside the heated cube. Therefore, the epoxy layer is represented by 5 grid points only.

On a non-uniform grid like this various ways exist to discretise the convective and diffusive operators in the Navier-Stokes equations (and the energy equation). We have applied a high-order, finite-volume discretisation method that preserves the spectral properties of the convective and diffusive operators, *i.e.* convection $\leftrightarrow$ skew-symmetric; diffusion $\leftrightarrow$ symmetric, positive definite.

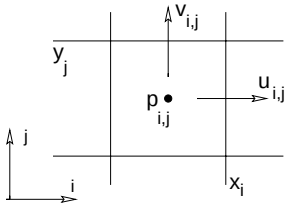

Figure 3: The location of the discrete velocities.

3.1 Basic idea

In this section we will sketch the main lines of such a symmetry-preserving discretisation in two spatial dimensions. The extension to 3D is straightforward. We will use the same notations as in the paper by Harlow & Welsh [5]. Figure 3 illustrates the definition of the discrete velocities $(u_{i,j}, v_{i,j})$. The discrete pressure and the temperature are defined in the centre of the grid-cells.

For an incompressible fluid the mass of any control volume $[x_{i-1}, x_i] \times [y_{j-1}, y_j]$ is conserved:

$$\bar{u}_{i,j} + \bar{v}_{i,j} - \bar{u}_{i-1,j} - \bar{v}_{i,j-1} = 0, \tag{1}$$

where

$$\bar{u}_{i,j} = \int_{y_{j-1}}^{y_j} u(x_i, y, t) dy \quad \text{and} \quad \bar{v}_{i,j} = \int_{x_{i-1}}^{x_i} v(x, y_j, t) dx. \tag{2}$$

The (semi-)discretisation of the transport of momentum of a region $\Omega_{i+1/2,j} = [x_{i-1/2}, x_{i+1/2}] \times [y_{j-1}, y_j]$ becomes

$$\begin{aligned} |\Omega_{i+1/2,j}| \frac{\mathrm{d}u_{i,j}}{\mathrm{d}t} &+ \bar{u}_{i+1/2,j} u_{i+1/2,j} + \bar{v}_{i+1/2,j} u_{i,j+1/2} \\ &- \bar{u}_{i-1/2,j} u_{i-1/2,j} - \bar{v}_{i+1/2,j-1} u_{i,j-1/2}. \end{aligned} \tag{3}$$

The non-integer indices in (3) refer to the faces of $\Omega_{i+1/2,j}$. For example, $u_{i-1/2,j}$ stands for the u-velocity at the interface of $\Omega_{i-1/2,j}$ and $\Omega_{i+1/2,j}$. The velocity at a control face is approximated by the average of the velocity at both sides of it:

$$u_{i+1/2,j} = \tfrac{1}{2}(u_{i+1,j} + u_{i,j}) \quad \text{and} \quad u_{i,j+1/2} = \tfrac{1}{2}(u_{i,j+1} + u_{i,j}). \tag{4}$$

In addition to the set of equations for the u-component of the velocity (3)-(4), there is an analoguous set for the v-component.

We conceive Eqs. (3)-(4) (and the analoguous set for v) as expressions for the velocities, where the mass fluxes $\bar{u}$ and $\bar{v}$ form the coefficients. Thus, we can write the discretisation in matrix-vector notation as

$$\boldsymbol{\Omega}_1 \frac{\mathrm{d}\boldsymbol{u}_h}{\mathrm{d}t} + \boldsymbol{C}_1(\bar{\boldsymbol{u}})\boldsymbol{u}_h, \tag{5}$$

where $\boldsymbol{u}_h$ denotes the discrete velocity-vector (which consists of both the $u_{i,j}$'s and $v_{i,j}$'s), $\boldsymbol{\Omega}_1$ is a (positive-definite) diagonal matrix representing the sizes of the control volumes $|\Omega_{i+1/2,j}|$ and $|\Omega_{i,j+1/2}|$, whereas $\boldsymbol{C}_1$ is built from the flux contributions through the control faces, *i.e.* $\boldsymbol{C}_1$ depends on the mass fluxes $\bar{u}$ and $\bar{v}$ at the control faces.

On a non-uniform grid one would be tempted to tune the weights $\frac{1}{2}$ in the interpolations given by (4) to the actual mesh sizes, but we think that it is important that the skew-symmetry of the underlying differential operator is preserved. The preservation of properties of differential operators forms in itself a reason for discretising them in a certain manner. We give it a concrete form by noting that the discrete transport equation

$\boldsymbol{\Omega}_1\dot{\boldsymbol{u}}_h + \boldsymbol{C}_1\boldsymbol{u}_h = \boldsymbol{0}$ conserves the discrete energy $\boldsymbol{u}_h^*\boldsymbol{\Omega}_1\boldsymbol{u}_h$ (for any discrete velocity field $\boldsymbol{u}_h$) if and only if the matrix $\boldsymbol{C}_1$ is skew-symmetric:

$$\frac{\mathrm{d}}{\mathrm{d}t}\left(\boldsymbol{u}_h^*\boldsymbol{\Omega}_1\boldsymbol{u}_h\right) = -\boldsymbol{u}_h^*\left(\boldsymbol{C}_1 + \boldsymbol{C}_1^*\right)\boldsymbol{u}_h = 0 \iff \boldsymbol{C}_1 + \boldsymbol{C}_1^* = \boldsymbol{0}$$

The matrix $\boldsymbol{C}_1 - \mathrm{diag}(\boldsymbol{C}_1)$ is skew-symmetric if and only if the weights in (4) are taken constant. Indeed, for $\boldsymbol{C}_1 - \mathrm{diag}(\boldsymbol{C}_1)$ to be a skew-symmetric matrix, the flux $\bar{v}_{i+1/2,j}u_{i,j+1/2}$ through the surface $y = y_j$ of the control volumes for $u_{i,j}$ and $u_{i,j+1}$ has to be computed independent of the control volume in which it is considered. This can only be achieved when the weights in the interpolation (4) are taken independent of the grid location (and hence equal to the uniform weights). Otherwise, the skew-symmetric of $\boldsymbol{C}_1 - \mathrm{diag}(\boldsymbol{C}_1)$ is lost. Therefore, we take constant weights in (4), also on non-uniform grids.

In the notation above, we have suppresed the argument $\bar{\boldsymbol{u}}$ of $\boldsymbol{C}_1$, because $\boldsymbol{C}_1 - \mathrm{diag}(\boldsymbol{C}_1)$ is skew-symmetric for all $\bar{\boldsymbol{u}}$. The interpolation rule for the mass fluxes $\bar{u}$ and $\bar{v}$ through the faces of the control volumes is determined by the requirement that the diagonal of $\boldsymbol{C}_1$ has to be zero. Then, we have $\boldsymbol{C}_1 + \boldsymbol{C}_1^* = 0$. By substituting (4) into (3) we obtain the diagonal-element

$$\tfrac{1}{2}\left(\bar{u}_{i+1/2,j} + \bar{v}_{i+1/2,j} - \bar{u}_{i-1/2,j} - \bar{v}_{i+1/2,j-1}\right).$$

This expression is equal to a linear combination of left-hand sides of Eq. (1) if the mass fluxes in (3) are interpolated to the faces of a u-cell according to

$$\bar{u}_{i+1/2,j} = \tfrac{1}{2}(\bar{u}_{i+1,j} + \bar{u}_{i,j}) \quad \text{and} \quad \bar{v}_{i+1/2,j} = \tfrac{1}{2}(\bar{v}_{i+1,j} + \bar{v}_{i,j}). \tag{6}$$

It goes without saying that this interpolation rule is also applied in the j-direction to approximate the flux through the faces of v-cells.

So, in conclusion, the coefficient matrix $\boldsymbol{C}_1$ is skew-symmetric if Eq. (1) holds, and the discrete velocities $\boldsymbol{u}_h$ and mass fluxes $\bar{\boldsymbol{u}}$ are interpolated to the surfaces of control cells with constant coefficients.

In the continuous case diffusion corresponds to a symmetric, positive-definite operator. In our approach we want this property to hold also for the discrete operator. To obtain such a discretisation the normal derivative of a velocity at a control face may be approximated by the difference between the nearest velocities at both sides of the face divided by the distance between these discrete velocities. We denote the resulting coefficient matrix of the discretisation of the diffusive flux by $\boldsymbol{D}_1$.

Of course, we have to approximate the flux-vector $\bar{\boldsymbol{u}}$ in terms of the discrete velocity-vector $\boldsymbol{u}_h$ in order to close the discrete system of equations. The coefficient matrix $\boldsymbol{C}_1$ becomes then a function of the discrete velocity $\boldsymbol{u}_h$. The way in which the flux $\bar{\boldsymbol{u}}$ is approximated does not alter the skew-symmetry of $\boldsymbol{C}_1$: the matrix $\boldsymbol{C}_1$ is skew-symmetric for any relation between $\bar{\boldsymbol{u}}$ and $\boldsymbol{u}_h$. We apply the mid-point rule to approximate the mass fluxes $\bar{u}_{i,j}$ and $\bar{v}_{i,j}$:

$$\bar{u}_{i,j} = (y_j - y_{j-1})u_{i,j} \quad \text{and} \quad \bar{v}_{i,j} = (x_i - x_{i-1})v_{i,j}. \tag{7}$$

Then, the continuity equation (1) may be written in terms of the discrete velocity vector $\boldsymbol{u}_h$. We will denote the coefficient matrix by $\boldsymbol{M}_1$. Hence, the discretisation of the continuity equation reads $\boldsymbol{M}_1\boldsymbol{u}_h = \boldsymbol{0}$.

3.2 Higher-order, symmetry-preserving approximation

To turn Eq. (3) into a higher-order approximation, we write down the transport of momentum of a region $\Omega^{(3)}_{i+1/2,j} = [x_{i-3/2}, x_{i+3/2}] \times [y_{j-2}, y_{j+1}]$. Here, it may be noted that we cannot blow up the 'original' volumes $\Omega_{i+1/2,j}$ by a factor of two (in all directions) since our grid is not collocated. On a staggered grid, three times larger volumes are the smallest ones possible for which the same discretisation rules can be applied as for the 'original' volumes. This yields

$$\begin{aligned} |\Omega^{(3)}_{i+1/2,j}|\frac{\mathrm{d}u_{i,j}}{\mathrm{d}t} &+ \bar{\bar{u}}_{i+3/2,j}u_{i+3/2,j} + \bar{\bar{v}}_{i+1/2,j+1}u_{i,j+3/2} \\ &- \bar{\bar{u}}_{i-3/2,j}u_{i-3/2,j} - \bar{\bar{v}}_{i+1/2,j-2}u_{i,j-3/2}, \end{aligned} \tag{8}$$

where

$$\bar{\bar{u}}_{i,j} = \int_{y_{j-2}}^{y_j+1} u(x_i, y, t)dy \quad \text{and} \quad \bar{\bar{v}}_{i,j} = \int_{x_{i-2}}^{x_i+1} v(x, y_j, t)dy.$$

The velocities at the control faces of the large volumes are interpolated to the control faces in a way similar to that given by (4):

$$u_{i+3/2,j} = \tfrac{1}{2}(u_{i+3,j} + u_{i,j}) \quad \text{and} \quad u_{i,j+3/2} = \tfrac{1}{2}(u_{i,j+3} + u_{i,j}). \tag{9}$$

We conceive Eq. (8) as an expression for the velocities, where the surface integrals $\bar{\bar{u}}$ and $\bar{\bar{v}}$ form the coefficients. Considering it like that, we can recapitulate the equations above (together with the analoguous set for the v-component) by

$$\boldsymbol{\Omega}_3\frac{\mathrm{d}\boldsymbol{u}_h}{\mathrm{d}t} + \boldsymbol{C}_3(\bar{\bar{\boldsymbol{u}}})\boldsymbol{u}_h, \tag{10}$$

where the diagonal matrix $\boldsymbol{\Omega}_3$ represents the sizes of the large control volumes and $\boldsymbol{C}_3$ consists of flux contributions ($\bar{\bar{u}}$ and $\bar{\bar{v}}$) through the faces of these volumes.

On a uniform grid the local truncation errors in (5) and (10) are of the order $2+d$, where $d = 2$ in two spatial dimensions and $d = 3$ in 3D. The leading term in the discretisation error may be removed through a Richardson extrapolation (see *e.g.* [6]). This leads to the fourth-order approximation

$$\boldsymbol{\Omega}\frac{\mathrm{d}\boldsymbol{u}_h}{\mathrm{d}t} + \left(3^{2+d}\boldsymbol{C}_1(\bar{\boldsymbol{u}}) - \boldsymbol{C}_3(\bar{\bar{\boldsymbol{u}}})\right)\boldsymbol{u}_h,$$

where $\boldsymbol{\Omega} = 3^{2+d}\boldsymbol{\Omega}_1 - \boldsymbol{\Omega}_3$. The coefficient matrix of the convective operator depends on both $\bar{\boldsymbol{u}}$ and $\bar{\bar{\boldsymbol{u}}}$, since it is constructed out of $\boldsymbol{C}_1$ and $\boldsymbol{C}_3$. The diffusive term of the Navier-Stokes

equations undergoes a similar treatment. This leads to a fourth-order coefficient matrix $\boldsymbol{D} = 3^{2+d}\boldsymbol{D}_1 - \boldsymbol{D}_3$ where the symmetric, positive definite matrix $\boldsymbol{D}_3$ is the coefficient matrix of the discretisation of the diffusive flux through the faces of 3^d-times larger control volumes.

To eliminate the leading term of the discretisation error in the continuity equation, we apply the law of conservation of mass to $\Omega_{i,j}^{(3)} = [x_{i-2}, x_{i+1}] \times [y_{j-2}, y_{j+1}]$:

$$\bar{\bar{u}}_{i+1,j} + \bar{\bar{v}}_{i,j+1} - \bar{\bar{u}}_{i-2,j} - \bar{\bar{v}}_{i,j-2} = 0. \tag{11}$$

As noted before, the matrix $\boldsymbol{C}_1 - \mathrm{diag}(\boldsymbol{C}_1)$ is skew-symmetric, because the velocities at the control faces are interpolated with constant coefficients. The same holds for $\boldsymbol{C}_3$. The matrix $\boldsymbol{C}_3 - \mathrm{diag}(\boldsymbol{C}_3)$ is skew-symmetric for all interpolations of $\bar{\bar{u}}$ and $\bar{\bar{v}}$ to the control faces, since the velocities at the control faces are interpolated with constant coefficients, see (9). Hence, without its diagonal the coefficient matrix $3^{2+d}\boldsymbol{C}_1(\bar{\boldsymbol{u}}) - \boldsymbol{C}_3(\bar{\bar{\boldsymbol{u}}})$ is skew-symmetric. The matrix $3^{2+d}\boldsymbol{C}_1(\bar{\boldsymbol{u}}) - \boldsymbol{C}_3(\bar{\bar{\boldsymbol{u}}})$ has diagonal-elements like

$$\begin{array}{cl} 3^{d+2} & \frac{1}{2}(\bar{u}_{i+1/2,j} + \bar{v}_{i+1/2,j} - \bar{u}_{i-1/2,j} - \bar{v}_{i+1/2,j-1}) \\ - & \frac{1}{2}(\bar{\bar{u}}_{i+3/2,j} + \bar{\bar{v}}_{i+1/2,j+1} - \bar{\bar{u}}_{i-3/2,j} - \bar{\bar{v}}_{i+1/2,j-2}). \end{array}$$

For skew-symmetry the interpolation of the $\bar{u}$'s, $\bar{v}$'s, $\bar{\bar{u}}$'s and $\bar{\bar{v}}$'s to the control faces has to be performed in such a way that the diagonal-elements of $3^{2+d}\boldsymbol{C}_1(\bar{\boldsymbol{u}}) - \boldsymbol{C}_3(\bar{\bar{\boldsymbol{u}}})$ become equal to zero, that is equal to linear combinations of (1) and (11). To achieve this, we interpolate $\bar{u}_{i+1/2,j}$ in the following manner

$$\bar{u}_{i+1/2,j} = \tfrac{1}{2}\alpha(\bar{u}_{i+1,j} + \bar{u}_{i,j}) + \tfrac{1}{2}(1-\alpha)(\bar{u}_{i+2,j} + \bar{u}_{i-1,j}), \tag{12}$$

where α is a constant, and interpolate $\bar{v}_{i+1/2,j}$, $\bar{\bar{u}}_{i+1/2,j}$ and $\bar{\bar{v}}_{i+1/2,j}$ likewise. We take $\alpha = 9/8$ because all interpolations are fourth-order accurate then (on a uniform grid). Note that we can not take $\alpha = 1$ here (as in Eq. (6)) since a Richardson extrapolation does not eliminate the leading term in the truncation error of $\bar{\bar{u}}_{i+1/2,j}$ and $\bar{\bar{v}}_{i+1/2,j}$.

The mass fluxes $\bar{\bar{u}}_{i,j}$ and $\bar{\bar{v}}_{i,j}$ are approximated, so that they can be expressed in terms of the discrete velocities $u_{i,j}$ and $v_{i,j}$, respectively:

$$\bar{\bar{u}}_{i,j} = (y_{j-1} - y_{j-2})u_{i,j} \quad \text{and} \quad \bar{\bar{v}}_{i,j} = (x_{i-1} - x_{i-2})v_{i,j}. \tag{13}$$

Hence, on a uniform grid, the mass fluxes $\bar{\bar{u}}_{i,j}$ and $\bar{\bar{v}}_{i,j}$ are approximated by means of the mid-point rule. In matrix-vector notation, we may summarise the discretisation of the law of conservation of mass applied to the volumes $\Omega_{i,j}^{(3)}$ by an expression of the form $\boldsymbol{M}_3\boldsymbol{u}_h = \boldsymbol{0}$. The fourth-order approximation of the law of conservation of mass reads

$$\boldsymbol{M}\boldsymbol{u}_h = (3^{2+d}\boldsymbol{M}_1 - \boldsymbol{M}_3)\boldsymbol{u}_h = \boldsymbol{0},$$

where the weights 3^{2+d} and -1 are to be used on non-uniform grids too, since otherwise the symmetry of the underlying differential operator is lost.

After that the interpolation rule (12) is applied, and the flux is expressed in terms of the discrete velocity like in (7) and (13), the coefficient matrix $3^{2+d}\boldsymbol{C}_1(\bar{\boldsymbol{u}}) - \boldsymbol{C}_3(\bar{\bar{\boldsymbol{u}}})$ becomes a function of the discrete velocity vector $\boldsymbol{u}_h$ only. We will denote that function by $\boldsymbol{C}(\boldsymbol{u}_h)$. Then, the symmetry-preserving discretisation of the incompressible Navier-Stokes equations becomes

$$\boldsymbol{\Omega}\frac{\mathrm{d}\boldsymbol{u}_h}{\mathrm{d}t} + \boldsymbol{C}(\boldsymbol{u}_h)\boldsymbol{u}_h + \boldsymbol{D}\boldsymbol{u}_h - \boldsymbol{M}^*\boldsymbol{p}_h = \boldsymbol{0} \qquad \boldsymbol{M}\boldsymbol{u}_h = 0, \tag{14}$$

where $\boldsymbol{p}_h$ represents the discrete pressure.

Without diffusion, the mass, momentum and kinetic energy of a flow are conserved analytically. These quantities are also conserved by the discrete formulation (14). The energy $\boldsymbol{u}_h^*\boldsymbol{\Omega}\boldsymbol{u}_h$ of any solution $\boldsymbol{u}_h$ of (14) evolves in time according to

$$\frac{\mathrm{d}}{\mathrm{d}t}(\boldsymbol{u}_h^*\boldsymbol{\Omega}\boldsymbol{u}_h) = -\boldsymbol{u}_h^*(\boldsymbol{D} + \boldsymbol{D}^*)\boldsymbol{u}_h,$$

where the right-hand side is negative for all $\boldsymbol{u}_h \neq \boldsymbol{0}$ since $\boldsymbol{D}$ is a symmetric, positive-definite matrix. This implies that the semi-discrete system (14) is stable. Therefore a solution of (14) can be obtained on any grid (without adding artificial dissipation). Because stability is not an issue, the question becomes how accurate is this discretisation. Or, in other words, how coarse may the grid be?

3.3 Time-advancement

The time-advancement of the convective and diffusive fluxes in the air flow is carried out by an explicit one-leg method that is tuned to get the largest possible interval of convective stability, see [10]. The pressure p and the incompressibility constraint $\boldsymbol{M}\boldsymbol{u}_h = \boldsymbol{0}$ are treated implicitly in time. The energy equation is also integrated in time by means of a one-leg method. The temperature in the epoxy layer is updated by means of Euler's explicit method.

The diffusivity of air is approximately two orders of magnitude larger than that of epoxy. Consequently, the (diffusive) time scales in the air and in the epoxy layer differ significantly. Air reacts much faster upon temperature changes than epoxy does and it takes much longer to reach an equilibrium state in the epoxy layer than in the air. To shorten the time needed to reach an equilibrium the diffusivity in the epoxy layer is increased initially. It starts from a value that is slightly lower than the diffusivity of air and is then gradually decreased till it reaches its given value.

The thermal coupling has been implemented with the help of an overlap. That is we have defined a ghost air temperature at the centre of the first grid cell inside the heated cube and ghost epoxy temperature at the centre of the first grid cell outside the cube. At the interface both the temperature and the heat flux are continuous. These two conditions are discretised explicitly in time. Their spacial discretisation uses the ghost temperatures. From the two discretised boundary conditions we can solve the ghost epoxy temperature

in terms of non-ghost temperatures near the boundary. The resulting expression is stable, and thus the temperature in the epoxy layer can be updated in time. After that the air temperature is updated, where the ghost air temperature is computed from the Dirichlet condition at the boundary. Thus, the air and cube exchange temperatures and fluxes at their common boundary in an explicit, stable manner.

4 SIMULATION RESULTS

To validate our simulation code we have computed the velocity and the temperature of a fully developed flow in a channel with flat walls first. The results of this simulation are compared to those of several research groups in Section 4.1. The results for the channel with surface-mounted cubes can be found in Section 4.2.

4.1 A test-case: Plane channel flow

The plane channel is confined to a unit of dimension $2\pi \times 1 \times \pi$, where the height of the channel is normalised. This subdomain is covered by a $64 \times 64 \times 32$ staggered grid that is stretched away from the channel walls. The first grid point away from a wall is located at $4 \cdot 10^{-3}$. At the channel walls we have put the temperature equal to a constant. The Reynolds number is equal to $Re = 5,600$ (based on the channel width and the bulk velocity) and the Prandtl number is $Pr = 0.71$. At this Reynolds and Prandtl number a number of simulations have been performed by a several research groups; see *e.g.* [11], [12], [13] and [14].

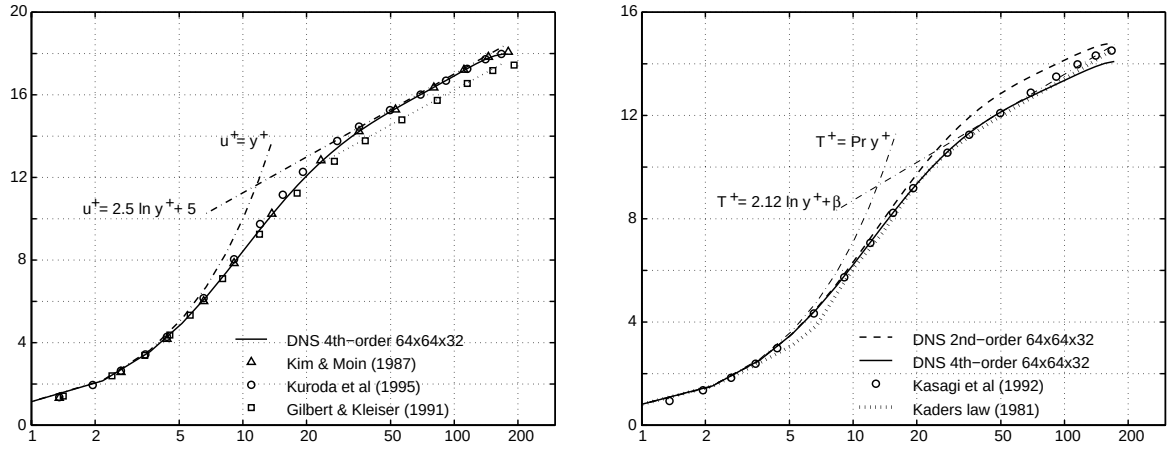

Figure 4: Comparison of the mean streamwise velocity u^+ (left) and mean temperature T^+ (right) as function of y^+ in a channel with flat walls. The dashed lines represent the law of the wall and the log law. The markers represent DNS-results that are taken from both the ERCOFTAC Database and the Japanese DNS Data Base of Turbulent Transport Phenomena. Kader's data provides the best fit through a large number of experiments (performed at a large range of Reynolds numbers).

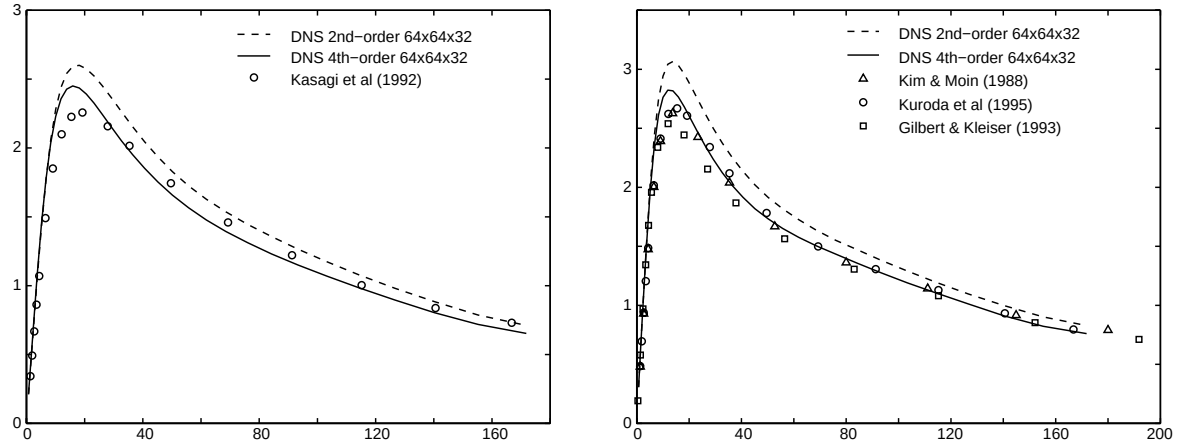

Figure 5: Comparison of the mean-square of the streamwise fluctuating velocity $\overline{u'u'}$ (left) and temperature $\overline{T'T'}$(right) as function of y^+ (linear scale) in a channel with flat walls.

Figure 4 shows a comparison of the mean velocity and mean temperature profiles as obtained from our fourth-order symmetry-preserving DNS with those of other DNS's. As usual, the profiles are made dimensionless with the friction velocity and friction temperature, respectively.

Here it may be stressed that the grids used by the DNS's that we compare with have typically about 128^3 grid points, that is 16 times more grid points than our grid has. Nevertheless, the agreement is excellent. This holds for the mean velocity as well as for the mean temperature. The agreement with Kader's formula [15] is also good. Thus, we may conclude that a $64 \times 64 \times 32$ grid suffices to perform this direct numerical simulation.

Figure 5 displays the fluctuating part of the velocity and temperture. The results shown in this figure affirm that the second-order method is less accurate than the fourth-order method. The can also be noted in Figure 4 (except for the mean velocity profile; in the mean velocity profile no difference can be noticed). Since the results of the second-order discretization method agree less with the reference data than those of the fourth-order method, we will use the fourth-order discretisation to simulate the flow and heat transfer in the channel with the surface mounted cubes.

4.2 Channel with surface mounted cubes

In this secion we will discuss some of the results of the simulation and will compare them to the available experimental data. The flow is computed on a 100^3 grid. The statistics have been averaged over 40 shedding cycles. The temporal behaviour of the flow is analysed with the help of a time series of the fluctuating streamwise velocity v' at a station in the wake of the cube The Strouhal number $St = 0.109$ obtained from this time series is exactly (in three digits) equal to that obtained from the experimental data. The Taylor micro-scale is approximately $5\,10^{-3}$ (non-dimensionalised by means of

the bulk velocity and the channel height). This value is also in good agreement with that determined from the experiments. In Fourier space the auto-correlation decays with a power of -1.55. The power density spectrum calculated from the experimental data decays with a power of approximately -1.6.

First- and second-order statistics of the velocity field obtained from the 100^3 DNS at the cross section of the channel that bisects a cube are compared to the available experimental data in Figure 6.

The profiles of the mean streamwise velocity and the mean-square of the fluctuating streamwise velocity are in good agreement with the experiments, except in the front of a cube, where some discrepancies between the mean-squares of the fluctuating streamwise velocities exist. So, in conclusion, the 100^3 simulation reproduces the turbulent flow fluctuations reasonably well. For a comparison with RaNS, we refer to [16].

Meinders *et al.* [8], [9] have measured the temperature at the surfaces of the heated cube by means of infrared thermography. At each face they have measured the surface temperature at a grid of 30^2 points. Liquid crystals were used to correct for the spatial image degradation of the infrared camera they used. Meinders *et al.* have calculated the radiative heat flux from the averaged measured temperature per face, the surface emissivity and the view factors of the faces. To determine the conductive heat flux at the outer surface of the epoxy layer, they have computed the temperature distribution inside the heated cube. For that, they solved the Laplace equation numerically on a 30^3 grid, where the temperature at the grid points on the faces was taken from the experiment.

Average temperatures and heat fluxes per face of the heated cube are compared in Table 1. Here, q_{cond} denotes the conductive heat flux through epoxy layer, q_{conv} represents the convective heat flux, and q_{rad} stands for the radiative heat flux. The average temperature per face is denoted by T_f. All quantities are given in the same physical dimensions as in the experiment. As can be seen the average surface temperatures of the simulation are lower than in the experiment. The largest difference occurs at the top face of the cube. There, the computed average surface temperature is approximately 7% lower than the measured temperature. The average temperatures at two side faces (side I and side II) of the cube should be equal by symmetry. The same applies to the fluxes at the two side faces. The experimental results do not satisfy the symmetry perfectly, due to errors in the measurements. The difference between the experimental results at the two side faces gives an idea of the magnitude of the error in the experiment.

The integral of the total heat flux ($q_{cond} = q_{conv} + q_{rad}$) over the five faces of the cube is $2.67W$ according to the measurements and $2.74W$ in the numerical simulation. The total power dissipated in the cube during the experiment was $2.96W$. Thus, the loss through the base at which the cube is mounted $(2.96 - 2.67W)$ is approximately four times the difference between the total heat flux in the experiment and in the numerical simulation.

The time-averaged temperatures along some paths at the surface of the heated cube are compared to those of the experiment in Figure 7. A number of measuring-points lie on the intersection of two paths. At these points two data-points are available. Both

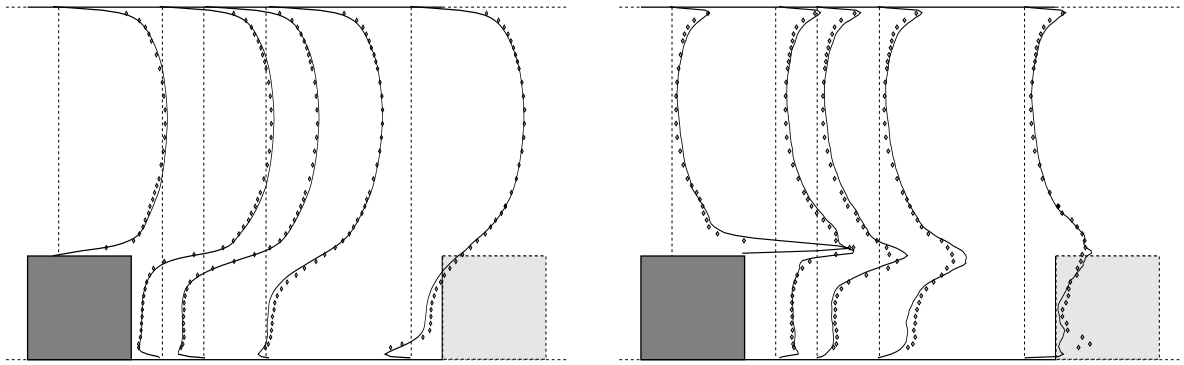

Figure 6: A comparison of first-order statistics (left handside picture) and second-order statistics (right handside) of the DNS with experimental data. Shown are the mean streamwise velocity $\overline{u}$ (left) and $\overline{u'u'}$ (right) in the plane parallel to the streamwise direction that bisects the cubes. The continuous lines correspond to the DNS; the experimental data is depicted by the dots.

	experiment				simulation			
face	q_{cond} W/m^2	q_{conv} W/m^2	q_{rad} W/m^2	T_f ^oC	q_{cond} W/m^2	q_{conv} W/m^2	q_{rad} W/m^2	T_f ^oC
windward	2976	2762	214.4	51.50	2775	2581	193.6	48.44
top	2592	2364	227.9	53.35	2687	2486	201.3	49.51
leeward	2084	1821	262.6	57.95	1717	1466	251.0	56.18
side I	2676	2445	230.6	53.74	2505	2295	210.1	50.73
side II	2597	2363	234.3	54.23	2505	2295	210.1	50.73

Table 1: Averaged heat fluxes and temperatures per cube face. A comparison of numerical results with experimental data.

are shown in Figure 7 to illustrate the uncertainty in the experimental data. Given this uncertainty, we may conclude that the experimentally and numerically obtained mean temperature agree.

Yet, at the edges the numerical simulation predicts a temperature that is lower than the measured temperature. The difference may become as large as five degrees, which is about 10%.

The distinct spatial gradients in the temperature distribution at the surface of the heated cube are related to the complex flow patterns near the cube. Obviously, the temperature at the windward face is low compared to that at the other faces. At the leeward face, the temperture is high because a large fraction of the heat is detained in the recirculation bubbles in the wake of the cube. Heat convected away from the cube recirculates in the wake and thus causes an increase of the temperature at the rear side of the cube, which in its turn suppresses the transfer of heat from the rear side. This

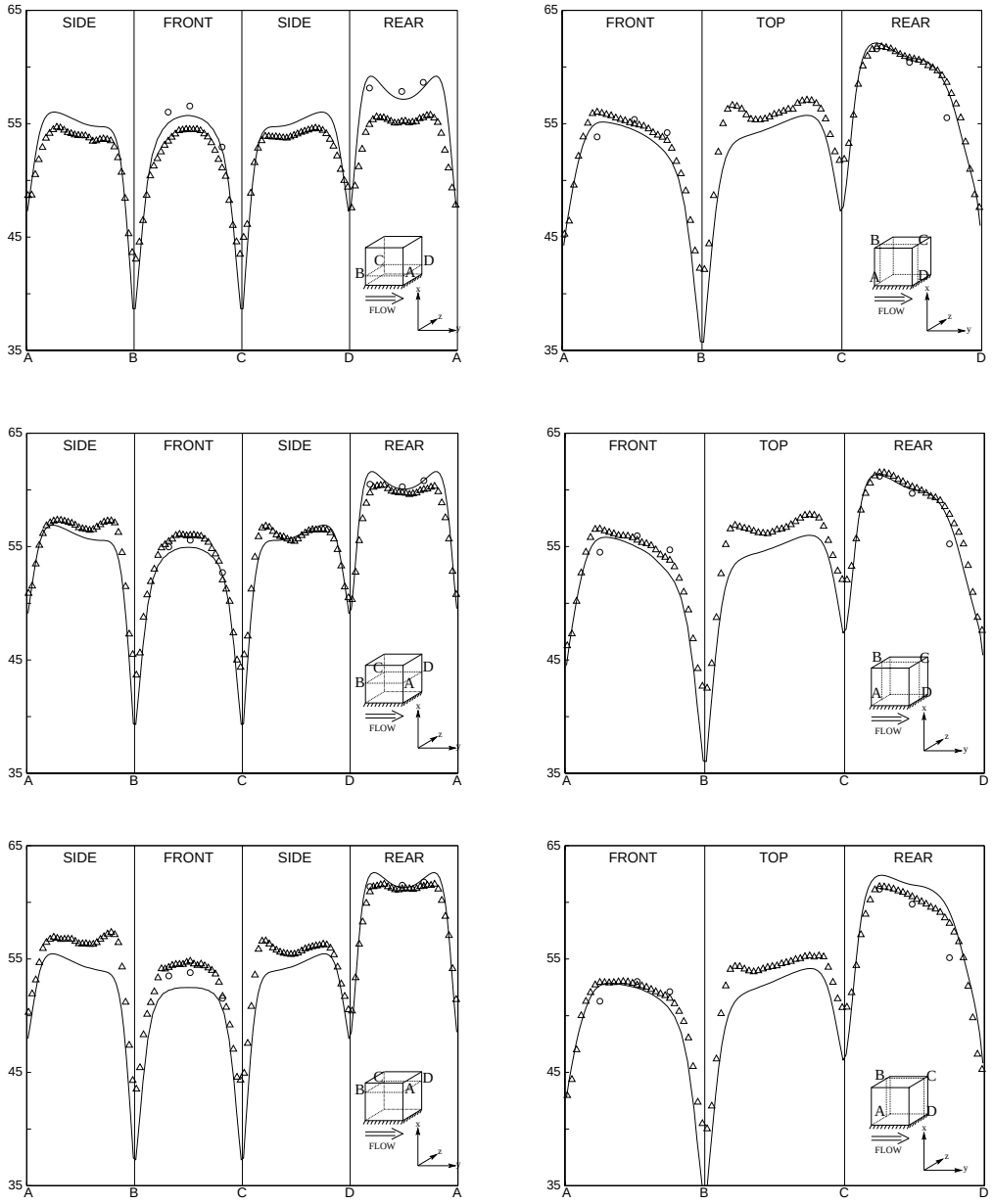

Figure 7: The mean temperature along different paths at the surface of the heated cube. The markers denote the experimental data by Meinders *et al.* Note that at three points along BC and DA (left-hand column) and at three points along AB and CD (right-hand column) two data-points are available. Both are shown.

phenomenon can also be observed at a smaller scale. For example, the distance between the corner B and the location of the maxima of the temperture at the path AB in the pictures in the left-hand column of Figure 7 is equal to the recirculation length along AB. In other words, the increase of the temperatures at the side face near the corner B is caused by an eddy that reduces the removal of heat from this part of the surface.

5 CONCLUSIONS

In this paper we have discussed the results of a symmetry-preserving simulation method for computing the flow and heat transfer in a channel with surface mounted cubical obstacles. The results can be summarised as follows.

- For a channel with flat walls the results of the fourth-order, symmetry-preserving discretisation method agree better with the reference data than those of the second-order method. With the fourth-order method a $64 \times 64 \times 32$ grid suffices to perform a DNS at $Re = 5,600$ (based on channel height and bulk velocity).

- The fourth-order, symmetry-preserving discretisation method yields good results for the flow and heat transfer in the channel with the surface mounted cubical obstacles. The turbulent flow profiles agree well with the available experimental data. The same holds for the time-averaged surface temperatures, except for the edges of the cube where differences up to 10% exist.

Acknowledgements

The Stichting Nationale Computerfaciliteiten (National Computing Facilities Foundation, NCF) with financial support from the Netherlands Organization for Scientific Research (NWO) is gratefully acknowledged for the use of supercomputer facilities.

REFERENCES

[1] K. Hanjalić and S. Obi (eds.), *Proceedings of the 6th ERCOFTAC/IAHR/COST Workshop on Refined Flow Modeling*, Delft University of Technology, The Netherlands (1997).

[2] T. Craft (ed.), *Proceedings of the 7th ERCOFTAC/IAHR/COST Workshop on Refined Flow Modeling*, UMIST, Manchester, UK (1998).

[3] A. Hellsten and P. Rautaheimo (eds.), *Proceedings of the 8th ERCOFTAC/IAHR/COST Workshop on Refined Flow Modeling*, Helsinki University of Technology, Finland (1999).

[4] A.E.P. Veldman and K. Rinzema, Playing with nonuniform grids, *J. Engng. Math* **26**, 119–130 (1991).

[5] F.H. Harlow and J.E. Welsh, Numerical calculation of time-dependent viscous incompressible flow of fluid with free surface, *Phys. Fluids* **8**, 2182–2189 (1965).

[6] M. Antonopoulos-Domis, Large-eddy simulation of a passive scalar in isotropic turbulence, *J. Fluid Mech.* **104**, 55–79 (1981).

[7] Y. Morinishi, T.S. Lund, O.V. Vasilyev and P. Moin, Fully conservative higher order finite difference schemes for incompressible flow, *J. Comp. Phys.* **143**, 90-124 (1998).

[8] E.R. Meinders, *Experimental study of heat transfer in turbulent flows over wall-mounted cubes*, Ph.D-thesis, Delft University of Technology (1998).

[9] E.R. Meinders, Th.H. van der Meer, K. Hanjalić and C.J.M. Lasance, Application of infrared thermography to the evaluation of local convective heat transfer on arrays of cubical protrusions, *Int. J. Heat and Fluid Flow* **18**, 152 (1997).

[10] R.W.C.P. Verstappen and A.E.P. Veldman, Direct numerical simulation of turbulence at lower costs, *J. Engng. Math.* **32**, 143–159 (1997).

[11] J. Kim, P. Moin and R. Moser, Turbulence statistics in fully developed channel flow at low Reynolds number, *J. Fluid Mech.* **177**, 133–166 (1987).

[12] N. Gilbert and L. Kleiser, Turbulence model testing with the aid of direct numerical simulation results, in *Proc. Turb. Shear Flows 8*, Paper 26-1, Munich (1991).

[13] N. Kasagi, Y. Tomita and A. Kuroda, Direct numerical simulation of passive scalar field in a turbulent channel flow, *ASME J. Heat Transfer* **114**, 598 (1992).

[14] A. Kuroda, N. Kasagi and M. Hirata, Direct numerical simulation of turbulent plane Couette-Poisseuille flows: effect of mean shear rate on the near-wall turbulence structures, in: *Proc Turb. Shear Flows 9*, F. Durst *et al.* (eds.), Berlin: Springer-Verlag 241-257 (1995).

[15] B.A. Kader, Temperature and concentration profiles in fully turbulent boundary layers, *Int. J. Heat Mass Transfer* **24**, 1541 (1981).

[16] R.W.C.P. Verstappen and A.E.P. Veldman, Spectro-consistent discretization of Navier-Stokes: a challenge to RANS and LES, *J. Engng. Math.* **34**, 163–179 (1998).